PHYSICAL REVIEW C **91**, 051301(R) (2015)

Accurate nuclear radii and binding energies from a chiral interaction

A. Ekström,[1,2] G. R. Jansen,[2,1] K. A. Wendt,[1,2] G. Hagen,[2,1] T. Papenbrock,[1,2] B. D. Carlsson,[3] C. Forssén,[3,1,2] M. Hjorth-Jensen,[4,5] P. Navrátil,[6] and W. Nazarewicz[4,2,7]

[1]*Department of Physics and Astronomy, University of Tennessee, Knoxville, Tennessee 37996, USA*
[2]*Physics Division, Oak Ridge National Laboratory, Oak Ridge, Tennessee 37831, USA*
[3]*Department of Fundamental Physics, Chalmers University of Technology, SE-412 96 Göteborg, Sweden*
[4]*Department of Physics and Astronomy and NSCL/FRIB Laboratory, Michigan State University, East Lansing, Michigan 48824, USA*
[5]*Department of Physics, University of Oslo, N-0316 Oslo, Norway*
[6]*TRIUMF, 4004 Wesbrook Mall, Vancouver, British Columbia, V6T 2A3 Canada*
[7]*Faculty of Physics, University of Warsaw, Pasteura 5, 02-093 Warsaw, Poland*

(Received 5 December 2014; revised manuscript received 10 April 2015; published 1 May 2015)

With the goal of developing predictive *ab initio* capability for light and medium-mass nuclei, two-nucleon and three-nucleon forces from chiral effective field theory are optimized simultaneously to low-energy nucleon-nucleon scattering data, as well as binding energies and radii of few-nucleon systems and selected isotopes of carbon and oxygen. Coupled-cluster calculations based on this interaction, named $\mathrm{NNLO_{sat}}$, yield accurate binding energies and radii of nuclei up to ^{40}Ca, and are consistent with the empirical saturation point of symmetric nuclear matter. In addition, the low-lying collective $J^\pi = 3^-$ states in ^{16}O and ^{40}Ca are described accurately, while spectra for selected p- and sd-shell nuclei are in reasonable agreement with experiment.

DOI: 10.1103/PhysRevC.91.051301 PACS number(s): 21.30.−x, 21.10.−k, 21.45.−v, 21.60.De

Introduction. Interactions from chiral effective field theory (EFT) [1–4] and modern applications of renormalization group techniques [5–8] have opened the door for a description of atomic nuclei consistent with the underlying symmetries of quantum chromodynamics, the theory of the strong interaction. Chiral nuclear forces can be constructed systematically from long-range pion physics augmented by contact interactions. Over the past decade, the renaissance of nuclear theory based on realistic nuclear forces and powerful computational methods has pushed the frontier of *ab initio* calculations from few-body systems and light nuclei [6,9,10] to medium-mass nuclei [11–19].

One of the main challenges in *ab initio* calculations is the accurate [20] reproduction of binding energies and radii of finite nuclei simultaneously with the empirical nuclear matter saturation point (binding energy per nucleon $E/A \approx 16$ MeV at the Fermi momentum $k_F \approx 1.33$ fm^{-1}) and incompressibility ($250 < K_0 < 315$ MeV [21]). For instance, lattice EFT calculations at next-to-next-to leading order (NNLO) employ a phenomenological four-nucleon contact force (a correction beyond NNLO) to counter the overbinding in nuclei heavier than ^{12}C [17], while the radii of ^{12}C and ^{16}O are still too small [22,23]. *Ab initio* calculations overbind medium-mass and heavy nuclei by about 1 MeV per nucleon, underestimate charge radii [24], and yield too-large separation energies [25]. The status of chiral-force predictions for binding energies and charge radii in finite nuclei is summarized in Fig. 1, with dark gray symbols representing the predictions of various state-of-the-art calculations. This is a serious shortcoming of current chiral Hamiltonians because it prevents theory from making accurate predictions when extrapolating to higher masses. The problem with the reproduction of nuclear matter saturation properties has been discussed extensively in the literature [26–39], and various solutions have been proposed, ranging from short-range correlations and Pauli blocking effects to the inclusion of many-body forces.

We start from the optimization of the chiral interaction at NNLO. Traditionally, one takes the pion-nucleon coupling constants c_i either from pion-nucleon scattering [47,48] or from peripheral partial waves in the nucleon-nucleon (NN) sector [49,50], while the remaining coupling constants [denoted "low-energy constants" (LECs)] are adjusted in the NN sector. The corresponding χ^2 optimizations consider scattering data up to laboratory energies of $T_{\mathrm{Lab}} \approx 350$ MeV. In a subsequent step, the remaining LECs of the leading three-nucleon (NNN) forces [51–53] are adjusted to data on $A \leqslant 4$ systems [40,54,55]. For details, we refer the reader to Refs. [2–4]. Hitherto such a strategy has not produced interactions that simultaneously describe bulk properties of both nuclei and nuclear matter [56].

Our optimization strategy is based on a different approach. Most importantly, we optimize NNN forces together with NN forces. This is consistent with the idea of EFT that improvements are made *order by order* and not nucleon by nucleon. The simultaneous optimization of NN and NNN forces is important because the long-range contributions of the NNN force contain LECs from pion-nucleon vertices that also enter the NN force. Moreover, in addition to low-energy NN data and the binding energies and charge radii of ^{3}H, ^{3,4}He, our set of fit observables also contains data on heavier nuclei; namely, binding energies and radii of carbon and oxygen isotopes. This is a major departure from the traditional approach that seeks to adjust LECs to data on few-body systems with $A = 2,3,4$ and then attempts to extrapolate to nuclei with $A \gg 1$ and to infinite nuclear matter. The following arguments motivate the strategy of including heavier nuclei into the optimization: First, no reliable experimental data constrain the isospin $T = 3/2$ components of the NNN force in nuclei with mass numbers $A = 3,4$ (see Refs. [57,58] for more discussion and prospects). Second, since our goal is to describe nuclear properties at low energies, LECs are adjusted

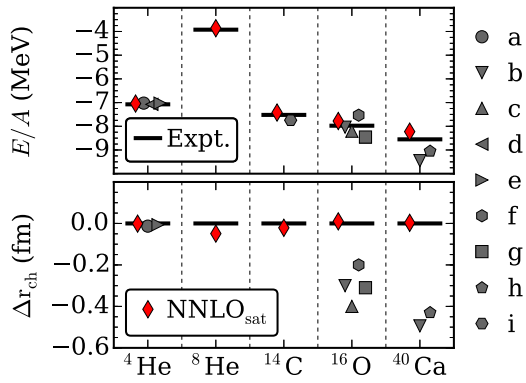

FIG. 1. (Color online) Ground-state energy (negative of binding energy) per nucleon (top), and residuals (differences between computed and experimental values) of charge radii (bottom) for selected nuclei computed with chiral interactions. In most cases, theory predicts too-small radii and too-large binding energies. References: *a* [40,41], *b* [24], *c* [23], *d* [22], *e* [42], *f* [43], *g* [44], *h* [45], *i* [46]. The red diamonds are $\mathrm{NNLO_{sat}}$ results obtained in this work.

to low-energy observables (as opposed to the traditional adjustment of two-nucleon forces to NN scattering data at higher energies). Third, the impact of many-body effects entering at higher orders (e.g., higher-rank forces) might be reduced if heavier systems, in which those effects are stronger, are included in the optimization.

Besides these theoretical arguments, there is also one practical reason for a paradigm shift: predictive power and large extrapolations do not go together. In traditional approaches, where interactions are optimized for $A = 2,3,4$, small uncertainties in few-body systems (e.g., by forcing a rather precise reproduction of the $A = 2,3,4$ sectors at a rather low order in the chiral power counting) get magnified tremendously in heavy nuclei; see, for example, Ref. [24]. Consequently, when aiming at reliable predictions for heavy nuclei, it is advisable to use a model that performs well for light- and medium-mass systems. In our approach, light nuclei are reached by interpolation while medium-mass nuclei by a modest extrapolation. In this context, it is worth noting that the most accurate calculations for light nuclei with $A \leqslant 12$ [59] employ NNN forces adjusted to 17 states in nuclei with $A \leqslant 8$ [60]. Finally, we point out that nuclear saturation can be viewed as an emergent phenomenon. Indeed, little in the chiral EFT of nuclear forces suggest that nuclei are self-bound systems with a central density (or Fermi momentum) that is practically independent of mass number. This viewpoint makes it prudent to include the emergent momentum scale into the optimization, which is done in our case by the inclusion of charge radii for ^{3}H, ^{3,4}He, ^{14}C, and ^{16}O. This is similar in spirit to nuclear mean-field calculations [61] and nuclear density functional theory [62,63] where masses and radii provide key constraints on the parameters of the employed models.

Optimization protocol and model details. We seek to minimize an objective function to determine the optimal set of coupling constants of the chiral $NN + NNN$ interaction at NNLO. Our dataset of fit-observables includes the binding energies and charge radii of ^{3}H, ^{3,4}He, ^{14}C, and ^{16}O, as well as binding energies of ^{22,24,25}O as summarized in Table I. To obtain charge radii r_{ch} from computed point-proton radii r_{pp} we use the standard expression [64]: $\langle r_{\mathrm{ch}}^2 \rangle = \langle r_{\mathrm{pp}}^2 \rangle + \langle R_{\mathrm{p}}^2 \rangle + \frac{N}{Z} \langle R_{\mathrm{n}}^2 \rangle + \frac{3\hbar^2}{4m_p^2 c^2}$, where $\frac{3\hbar^2}{4m_p^2 c^2} = 0.033$ fm^2 (Darwin–Foldy correction), $R_{\mathrm{n}}^2 = -0.1149(27)\,\mathrm{fm}^2$ [65], and $R_{\mathrm{p}} = 0.8775(51)$ fm [66]. In this work we ignore the spin-orbit contribution to charge radii [67]. From the NN sector, the objective function includes proton-proton and neutron-proton scattering observables from the SM99 database [68] up to 35 MeV scattering energy in the laboratory system as well as effective range parameters, and deuteron properties (see Table II). The maximum scattering energy was chosen such that an acceptable fit to both NN scattering data and many-body observables could be achieved.

In the present optimization protocol, the NNLO chiral force is tuned to low-energy observables. The comparison with the high-precision chiral NN interaction $\mathrm{N^3\,LO_{EM}}$ [49] and experimental data presented in Table II demonstrates the quality of $\mathrm{NNLO_{sat}}$ at low energies.

The results for ^{3}H and ^{3,4}He (and ^{6}Li) were computed with the no-core shell model (NCSM) [6,10] accompanied by infrared extrapolations [75]. The NNN force of $\mathrm{NNLO_{sat}}$ yields about 2 MeV of binding energy for ^{4}He. Heavier nuclei

TABLE I. Binding energies (in MeV) and charge radii (in fm) for ^{3}H, ^{3,4}He, ^{14}C, and ^{16,22,23,24,25}O employed in the optimization of $\mathrm{NNLO_{sat}}$.

	$E_{\mathrm{g.s.}}$	Expt. [69]	r_{ch}	Expt. [65,66]
^{3}H	8.52	8.482	1.78	1.7591(363)
^{3}He	7.76	7.718	1.99	1.9661(30)
^{4}He	28.43	28.296	1.70	1.6755(28)
^{14}C	103.6	105.285	2.48	2.5025(87)
^{16}O	124.4	127.619	2.71	2.6991(52)
^{22}O	160.8	162.028(57)		
^{24}O	168.1	168.96(12)		
^{25}O	167.4	168.18(10)		

TABLE II. Low-energy NN data included in the optimization. The scattering lengths a and effective ranges r are in units of fm. The proton-proton observables with superscript C include the Coulomb force. The deuteron binding energy (E_D, in MeV), structure radius (r_D, in fm), and quadrupole moment (Q_D, in fm^2) are calculated without meson-exchange currents or relativistic corrections. The computed d-state probability of the deuteron is 3.46%.

	$\mathrm{NNLO_{sat}}$	$\mathrm{N^3\,LO_{EM}}$ [49]	Expt.	Ref.
a_{pp}^C	−7.8258	−7.8188	−7.8196(26)	[70]
r_{pp}^C	2.855	2.795	2.790(14)	[70]
a_{nn}	−18.929	−18.900	−18.9(4)	[71]
r_{nn}	2.911	2.838	2.75(11)	[72]
a_{np}	−23.728	−23.732	−23.740(20)	[73]
r_{np}	2.798	2.725	2.77(5)	[73]
E_D	2.22457	2.22458	2.224566	[69]
r_D	1.978	1.975	1.97535(85)	[74]
Q_D	0.270	0.275	0.2859(3)	[73]

are computed with the coupled-cluster method (see Ref. [76] and the discussion below).

A total of 16 LECs determine the strengths of the NN contact potential, the πN potential in the $NN+NNN$ sector, and the NNN contacts. The LECs are constrained simultaneously by the optimization algorithm POUNDERS [63]. We employ standard nonlocal regulators in the construction of the potential; see, e.g., Refs. [49,52] for details. This type of regulator improves the convergence of nuclear matter calculations [56]. In detail, the regulator functions consist of exponentiated Jacobi momenta p divided by a cutoff value Λ, i.e., $\sim\exp[(p/\Lambda)^{2n}]$. For the present work, we set $n=3$ and $\Lambda=450$ MeV. Furthermore, the subleading two-pion exchange in the NN interaction is regularized by using spectral function regularization with a cutoff $\Lambda_{\rm SFR}=700$ MeV. The details of this procedure can be found in Refs. [77,78].

The objective function is numerically expensive, requiring us to adopt some approximations when computing nuclei with $A>4$. In the optimization, we employed a model space of nine oscillator shells for the NN interaction, the energy cutoff $E_{3\rm max}=8\hbar\Omega$ for the NNN forces, and the coupled-cluster method in its singles and doubles approximation (CCSD). We use nucleus-dependent estimates for larger model spaces and triples-cluster corrections based on Ref. [15]. During the optimization, we verified that these estimates were accurate by performing converged calculations. In our final computation of the objective function and for the results presented in this paper, we employ much larger model spaces and coupled-cluster methods with higher precision.

The coupled-cluster calculations are based on the intrinsic Hamiltonian $H=T-T_{\rm cm}+V_{NN}+V_{NNN}$ to minimize spurious center-of-mass effects [15,79,80]. For the binding energies presented in this paper we employ the Λ-CCSD(T) approximation [15,81,82] in a model space consisting of 15 oscillator shells with $\hbar\Omega=22$ MeV. The NNN forces are limited to an energy cutoff $E_{3\rm max}=16\hbar\Omega$ and truncated at the normal-ordered two-body level in the Hartree–Fock basis [83,84]. We also include the leading-order residual NNN contribution to the total energy as a second-order perturbative energy correction [56], computed with $E_{3\rm max}=12\hbar\Omega$.

To compute excited states in and around nuclei with closed shells, we employ equation-of-motion coupled-cluster methods [80,85–89]; these are accurate for excited states that are generalized particle-hole excitations of low rank. For instance, ^{14}N is computed with the charge-symmetry-breaking equation-of-motion method from the closed subshell nucleus ^{14}C; see Ref. [89]. Similar comments apply to ^{22,24}F. The intrinsic charge radii are computed from the two-body density matrix (2BDM) in the CCSD approximation [90]. Benchmark calculations of the ^{4}He charge radius shows that the 2BDM result is 1% larger than the NCSM result. Intrinsic charge densities are computed by using the one-body density matrix and correcting for the Gaussian center-of-mass wave function [76,91]. In the case of ^{16}O, this approach has been validated against 2BDM to four significant digits.

The values for the LECs that result from the optimization and define the chiral potential NNLO$_{\rm sat}$ are listed in Table III. We note that the pion-nucleon LECs c_1,c_3 and c_4 are in the range of the published values [48,49,92]. Following Ref. [49],

TABLE III. The values of the LECs for the NNLO$_{\rm sat}$ interaction. The constants c_i, $\tilde{C}_i$, and C_i are in units of GeV^{-1}, 10^4 GeV^{-2}, and 10^4 GeV^{-4}, respectively.

LEC	Value	LEC	Value	LEC	Value
c_1	−1.12152120	c_3	−3.92500586	c_4	3.76568716
$\tilde{C}_{^1S_0}^{pp}$	−0.15814938	$\tilde{C}_{^1S_0}^{np}$	−0.15982245	$\tilde{C}_{^1S_0}^{nn}$	−0.15915027
$C_{^1S_0}$	2.53936779	$C_{^3S_1}$	1.00289267	$\tilde{C}_{^3S_1}$	−0.17767436
$C_{^1P_1}$	0.55595877	$C_{^3P_0}$	1.39836559	$C_{^3P_1}$	−1.13609526
$C_{^3S_1-^3D_1}$	0.60071605	$C_{^3P_2}$	−0.80230030	c_D	0.81680589
c_E	−0.03957471				

we set the pion-decay constant $f_\pi=92.4$ MeV and the axial-vector coupling constant $g_A=1.29$. The value for g_A is greater than the experimental estimate $g_A=1.276$ [93] to account for the Goldberger–Treiman discrepancy. We use the following neutron, proton, and nucleon masses: $m_n=939.5653$ MeV, $m_p=938.272$ MeV, and $m_N=938.9184$ MeV, respectively. For the pion masses we use $m_{\pi^\pm}=139.5702$ MeV and $m_{\pi^0}=134.9766$ MeV. For the NN scattering data up to 35 MeV a total χ^2/datum ≈ 4.3 was reached. Representative phase shifts are shown in Fig. 2. The phase shifts at higher scattering energies demonstrates that NNLO$_{\rm sat}$ is at the limits of expectations one can have for an interaction at this chiral order. Furthermore, the accuracy of NNLO$_{\rm sat}$ in the few-body sector is similar to other chiral interactions at order NNLO [52,94].

Predictions. We begin with predictions for the β-decay half-life of ^{3}H. The reduced matrix element $|\langle^3\mathrm{He}||E_1^A||^3\mathrm{H}\rangle|=0.6343$ compares well to the corresponding experimental value of 0.6848 ± 0.0011 [55,96]. Figure 1 shows that binding energies and charge radii of the p-shell nuclei ^{8}He, ^{14}C, and ^{16}O are in good agreement with experiment. For ^{8}He the computed binding energy and charge radius are 30.9 MeV and 1.91 fm, respectively, and in good agreement with the experimental binding energy 31.5 MeV [69] and experimental charge radius 1.959(16) fm [97]. For ^{6,9}Li we compute a binding energy of 32.4(4) and 43.9 MeV, respectively, which compare well with experiment (32.0 and 45.34 MeV [69]). The charge radius of ^{9}Li with NNLO$_{\rm sat}$ is 2.22 fm; also consistent with the measured value of 2.217(35) fm [98]. We now discuss results for excited states in ^{6}Li, ^{14}C, ^{14}N, and ^{16}O; see Fig. 3. The nucleus ^{6}Li is difficult to compute because it is bound by only 1.5 MeV relative to the threshold for deuteron emission. Effects of continuum is expected to lower the 2^+ resonances significantly [99]; thus we conclude that our results are in reasonable agreement with experiment. We also compared the spectra computed in the NCSM and agreement with the coupled-cluster prediction is good. The binding energy computed from two-particle attached equation-of-motion method [80,87] is 30.9 MeV and in reasonable agreement with the NCSM extrapolated result 32.4(4) MeV. Our predictions for the excited states of ^{14}C and ^{14}N agree with experiment except for the 1_2^+ state in ^{14}N.

The *ab initio* computation of negative-parity states in ^{16}O, particularly the 3_1^- state at 6.13 MeV [23,43,104,105], has been a long-standing theoretical challenge. We computed this state,

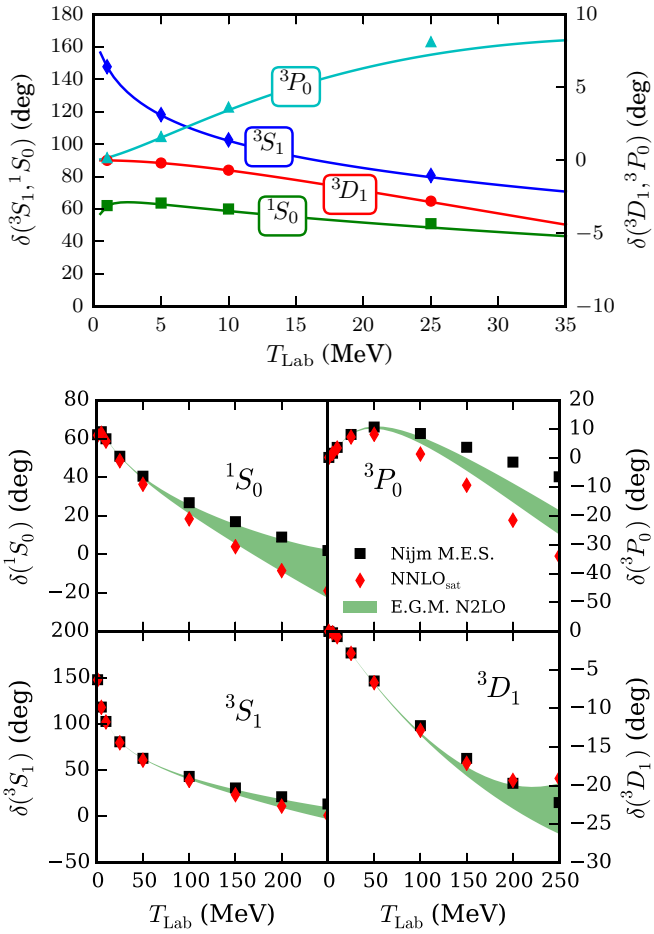

FIG. 2. (Color online) Selected neutron-proton scattering phase-shifts as a function of the laboratory scattering energy $T_{\rm Lab}$. (Top) NNLO$_{\rm sat}$ prediction (solid lines) compared to the Nijmegen phase shift analysis [95] (symbols) at low energies $T_{\rm Lab} < 35$ MeV. Note the two vertical scales. (Bottom) Neutron-proton scattering phase shifts from NNLO$_{\rm sat}$ (red diamonds) compared to the Nijmegen phase shift analysis (black squares) and the NNLO potentials (green) from Ref. [77].

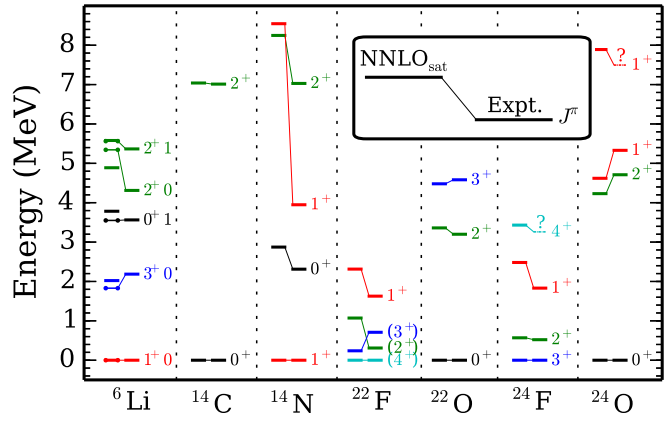

FIG. 3. (Color online) Energies (in MeV) of selected excited states for various nuclei using NNLO$_{\rm sat}$. For ^{6}Li we also include spectra from the NCSM (dotted lines), and isospin quantum numbers are also given. The NCSM results were obtained with $N_{\rm max} = 10$ and $\hbar\Omega = 16$ MeV. Parenthesis denote tentative spins assignments for experimental levels. Data are from Refs. [100–103].

dominated by about 90% of $1p$-$1h(p_{1/2} \rightarrow d_{5/2})$ excitations, at 6.34 MeV. The energy of the 3^-_1 state is strongly correlated with the charge radius of ^{16}O, with smaller charge radii leading to higher excitation energies. For $1p$-$1h$ excited states, the excitation energy depends on the particle-hole gap and therefore on one-nucleon separation energies of the $A = 16$ and $A = 17$ systems. The charge radius depends also on the proton separation energy S_p. For ^{16}O we find $S_p = 10.69$ MeV and the neutron separation energy $S_n(^{17}{\rm O}) = 4.0$ MeV, in an acceptable agreement with the experimental values of 12.12 and 4.14 MeV, respectively. For ^{17}F we find $S_p = 0.5$ MeV, to be compared with the experimental threshold at 0.6 MeV.

The inset of Fig. 4 shows that the 2^-_1 state in ^{16}O also comes out well, suggesting a $1p$-$1h$ nature. However, the 1^-_1 state is about 1.5 MeV too high compared with experiment. This state is dominated by $1p$-$1h$ excitations from the occupied $p_{1/2}$ to the unoccupied $s_{1/2}$ orbitals. In ^{17}O the $1/2^+$ state is computed at an excitation energy of 2.2 MeV, which is about 1.4 MeV too high. This probably explains the discrepancy observed for the 1^- state in ^{16}O.

Figure 4 shows that the experimental charge-density of ^{16}O is well reproduced with NNLO$_{\rm sat}$, and our charge form factor is, for momenta up to the second diffraction maximum, similar in quality to what Mihaila and Heisenberg [11] achieved with the Av18 + UIX potential. For the heavier isotopes ^{22,24}O and ^{22,24}F Fig. 3 shows good agreement between theory and experiment for excited states. For ^{22}F our computed spin assignments agree with results from shell-model Hamiltonians [106] and with recent *ab initio* results [89]. The binding energies for ^{14}N, ^{22,24}F are 103.7, 163, and 175.1 MeV, respectively, in good agreement with data (104.7, 167.7, and 179.1 MeV). We also computed the intrinsic charge (matter) radii of ^{22,24}O and obtained 2.72 fm (2.80 fm) and 2.76 fm (2.95 fm), respectively. The matter radius of ^{22}O agrees with the experimental result from Ref. [91]. We note that the computed spectra in ^{18}O is too

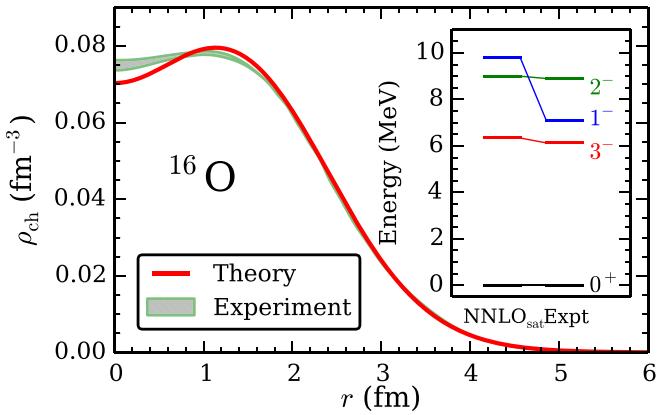

FIG. 4. (Color online) Charge density in ^{16}O computed as in Ref. [110] compared to the experimental charge density [111]. The inset compares computed low-lying negative-parity states with experiment.

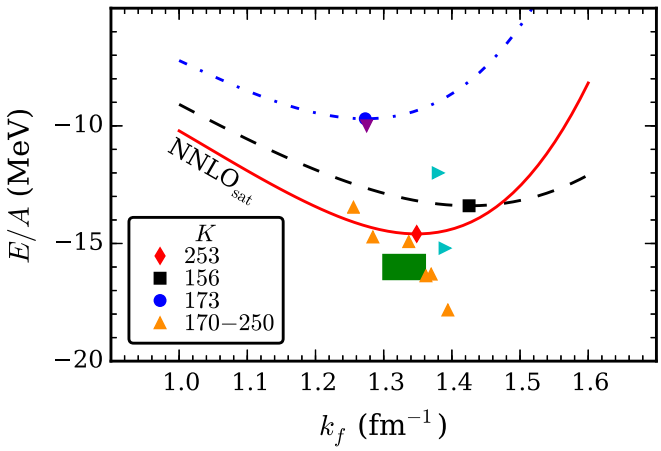

FIG. 5. (Color online) Equation of state for symmetric nuclear matter from chiral interactions. Solid red line is the prediction of NNLO$_{sat}$. Blue dashed-dotted and black dashed lines: Ref. [56]. Symbols (red diamond, blue circle, black square) mark the corresponding saturation points. Triangles are saturation points from other models (upward triangles [33], rightward triangles [112], downward triangles [36]). The corresponding incompressibilities (in MeV) are indicated by numbers. Green box shows empirical saturation point.

compressed compared to experiment (theory yields 0.7 MeV compared to 1.9 MeV for the first excited 2^+ state), possibly due to the too-high $1/2^+$ excited state in ^{17}O. In general, the quality of our spectra for *sd*-shell nuclei is comparable to those of recent state-of-the-art calculations with chiral Hamiltonians [44,107–109], while radii are much improved.

For ^{40}Ca the computed binding energy $E = 326$ MeV, charge radius $r_{ch} = 3.48$ fm, and $E(3_1^-) = 3.81$ MeV all agree well with the experimental values of 342 MeV, 3.4776(19) fm [65], and 3.736 MeV respectively. We checked that our energies for the 3_1^- states in ^{16}O and ^{40}Ca are practically free from spurious center-of-mass effects. The results for ^{40}Ca illustrate the predictive power of NNLO$_{sat}$ when extrapolating to medium-mass nuclei.

Finally, we present predictions for infinite nuclear matter. The accurate reproduction of the saturation point and incompressibility of symmetric nuclear matter has been a challenge for *ab initio* approaches, with representative results from chiral interactions shown in Fig. 5. The solid line shows the equation of state for NNLO$_{sat}$. Its saturation point is close to the empirical point, and its incompressibility $K = 253$ lies within the accepted empirical range [21]. At saturation density, coupled-cluster with doubles yields about 6 MeV per particle in correlation energy, while triples corrections (and residual NNN forces beyond the normal-ordered two-body approximation) yield another 1.5 MeV.

Let us briefly discuss the saturation mechanism. Similar to $V_{low\,k}$ potentials [5], the NN interaction of NNLO$_{sat}$ is soft and yields nuclei with too-large binding energies and too-small radii. The NNN interactions of NNLO$_{sat}$ are essential to arrive at physical nuclei, similarly to the role of NNN forces in the saturation of nuclear matter with low-momentum potentials [33]. This situation is reminiscent of the role the three-body terms play in nuclear density functional theory [113].

Summary. We have developed a consistently optimized interaction from chiral EFT at NNLO that can be applied to nuclei and infinite nuclear matter. Our guideline was the simultaneous optimization of NN and NNN forces to experimental data, including two-body and few-body data, as well as properties of selected light nuclei such as carbon and oxygen isotopes. The optimization is based on low-energy observables including binding energies and radii. The predictions made with the new interaction NNLO$_{sat}$ include accurate charge radii and binding energies. Spectra for ^{40}Ca and selected isotopes of lithium, nitrogen, oxygen and fluorine isotopes are well reproduced, as well as the energies of 3_1^- excitations in ^{16}O and ^{40}Ca. To our knowledge, NNLO$_{sat}$ is currently the only microscopically founded interaction that allows for a good description of nuclei (including their masses and radii) in a wide mass range from few-body systems to medium mass.

Acknowledgments. We thank K. Hebeler and E. Epelbaum for providing the matrix elements of the nonlocal three-body interaction. This material is based upon work supported by the U.S. Department of Energy, Office of Science, Office of Nuclear Physics under Award Numbers DEFG02-96ER40963 (University of Tennessee), DE-SC0008499 and DE-SC0008511 (NUCLEI SciDAC collaboration), the Field Work Proposal ERKBP57 at Oak Ridge National Laboratory and the National Science Foundation with award number 1404159. It was also supported by the Swedish Foundation for International Cooperation in Research and Higher Education (STINT, IG2012-5158), by the European Research Council (ERC-StG-240603), by the Research Council of Norway under contract ISP-Fysikk/216699, and by NSERC Grant No. 401945-2011. TRIUMF receives funding via a contribution through the National Research Council Canada. Computer time was provided by the Innovative and Novel Computational Impact on Theory and Experiment (INCITE) program. This research used resources of the Oak Ridge Leadership Computing Facility located in the Oak Ridge National Laboratory, which is supported by the Office of Science of the Department of Energy under Contract No. DE-AC05-00OR22725 and used computational resources of the National Center for Computational Sciences, the National Institute for Computational Sciences, the Swedish National Infrastructure for Computing (SNIC), and the Notur project in Norway.

[1] P. F. Bedaque and U. van Kolck, Annu. Rev. Nucl. Part. Sci. **52**, 339 (2002).

[2] E. Epelbaum, H.-W. Hammer, and U.-G. Meißner, Rev. Mod. Phys. **81**, 1773 (2009).

[3] R. Machleidt and D. Entem, Phys. Rep. **503**, 1 (2011).

[4] H.-W. Hammer, A. Nogga, and A. Schwenk, Rev. Mod. Phys. **85**, 197 (2013).

[5] S. K. Bogner, T. T. S. Kuo, and A. Schwenk, Phys. Rep. **386**, 1 (2003).

[6] P. Navrátil, S. Quaglioni, I. Stetcu, and B. R. Barrett, J. Phys. G: Nucl. Part. Phys. **36**, 083101 (2009).

[7] S. Bogner, R. Furnstahl, and A. Schwenk, Prog. Part. Nucl. Phys. **65**, 94 (2010).
[8] R. J. Furnstahl and K. Hebeler, Rep. Prog. Phys. **76**, 126301 (2013).
[9] S. C. Pieper and R. B. Wiringa, Annu. Rev. Nucl. Part. Sci. **51**, 53 (2001).
[10] B. R. Barrett, P. Navrátil, and J. P. Vary, Prog. Part. Nucl. Phys. **69**, 131 (2013).
[11] B. Mihaila and J. H. Heisenberg, Phys. Rev. Lett. **84**, 1403 (2000).
[12] D. J. Dean and M. Hjorth-Jensen, Phys. Rev. C **69**, 054320 (2004).
[13] G. Hagen, T. Papenbrock, D. J. Dean, and M. Hjorth-Jensen, Phys. Rev. Lett. **101**, 092502 (2008).
[14] C. Barbieri and M. Hjorth-Jensen, Phys. Rev. C **79**, 064313 (2009).
[15] G. Hagen, T. Papenbrock, D. J. Dean, and M. Hjorth-Jensen, Phys. Rev. C **82**, 034330 (2010).
[16] E. Epelbaum, H. Krebs, D. Lee, and U.-G. Meißner, Eur. Phys. J. A **45**, 335 (2010).
[17] T. A. Lähde, E. Epelbaum, H. Krebs, D. Lee, U.-G. Meißner, and G. Rupak, Phys. Lett. B **732**, 110 (2014).
[18] V. Somà, C. Barbieri, and T. Duguet, Phys. Rev. C **87**, 011303 (2013).
[19] H. Hergert, S. K. Bogner, S. Binder, A. Calci, J. Langhammer, R. Roth, and A. Schwenk, Phys. Rev. C **87**, 034307 (2013).
[20] In this Rapid Communication accuracy refers to an agreement with data at the precision one would expect from the model and method.
[21] J. R. Stone, N. J. Stone, and S. A. Moszkowski, Phys. Rev. C **89**, 044316 (2014).
[22] E. Epelbaum, H. Krebs, T. A. Lähde, D. Lee, and U.-G. Meißner, Phys. Rev. Lett. **109**, 252501 (2012).
[23] E. Epelbaum, H. Krebs, T. A. Lähde, D. Lee, U.-G. Meißner, and G. Rupak, Phys. Rev. Lett. **112**, 102501 (2014).
[24] S. Binder, J. Langhammer, A. Calci, and R. Roth, Phys. Lett. B **736**, 119 (2014).
[25] H. Hergert, S. K. Bogner, T. D. Morris, S. Binder, A. Calci, J. Langhammer, and R. Roth, Phys. Rev. C **90**, 041302 (2014).
[26] H. Müther and A. Polls, Prog. Part. Nucl. Phys. **45**, 243 (2000).
[27] H. Heiselberg and M. Hjorth-Jensen, Phys. Rep. **328**, 237 (2000).
[28] Y. Dewulf, W. H. Dickhoff, D. Van Neck, E. R. Stoddard, and M. Waroquier, Phys. Rev. Lett. **90**, 152501 (2003).
[29] W. Dickhoff and C. Barbieri, Prog. Part. Nucl. Phys. **52**, 377 (2004).
[30] F. Sammarruca, Int. J. Mod. Phys. E **19**, 1259 (2010).
[31] E. van Dalen and H. Müther, Int. J. Mod. Phys. E **19**, 2077 (2010).
[32] S. Krewald, E. Epelbaum, U.-G. Meißner, and P. Saviankou, Prog. Part. Nucl. Phys. **67**, 322 (2012).
[33] K. Hebeler, S. K. Bogner, R. J. Furnstahl, A. Nogga, and A. Schwenk, Phys. Rev. C **83**, 031301 (2011).
[34] M. B. Tsang, J. R. Stone, F. Camera, P. Danielewicz, S. Gandolfi, K. Hebeler, C. J. Horowitz, J. Lee, W. G. Lynch, Z. Kohley *et al.*, Phys. Rev. C **86**, 015803 (2012).
[35] G. Baardsen, A. Ekström, G. Hagen, and M. Hjorth-Jensen, Phys. Rev. C **88**, 054312 (2013).
[36] A. Carbone, A. Polls, and A. Rios, Phys. Rev. C **88**, 044302 (2013).
[37] M. Kohno, Phys. Rev. C **88**, 064005 (2013).
[38] K. Hebeler, J. M. Lattimer, C. J. Pethick, and A. Schwenk, Astrophys. J. **773**, 11 (2013).
[39] A. M. Shirokov, A. G. Negoita, J. P. Vary, S. K. Bogner, A. I. Mazur, E. A. Mazur, and D. Gogny, Phys. Rev. C **90**, 024324 (2014).
[40] P. Navrátil, V. G. Gueorguiev, J. P. Vary, W. E. Ormand, and A. Nogga, Phys. Rev. Lett. **99**, 042501 (2007).
[41] E. D. Jurgenson, P. Navrátil, and R. J. Furnstahl, Phys. Rev. C **83**, 034301 (2011).
[42] P. Maris, J. P. Vary, A. Calci, J. Langhammer, S. Binder, and R. Roth, Phys. Rev. C **90**, 014314 (2014).
[43] M. Włoch, D. J. Dean, J. R. Gour, M. Hjorth-Jensen, K. Kowalski, T. Papenbrock, and P. Piecuch, Phys. Rev. Lett. **94**, 212501 (2005).
[44] G. Hagen, M. Hjorth-Jensen, G. R. Jansen, R. Machleidt, and T. Papenbrock, Phys. Rev. Lett. **108**, 242501 (2012).
[45] S. Bacca, N. Barnea, G. Hagen, M. Miorelli, G. Orlandini, and T. Papenbrock, Phys. Rev. C **90**, 064619 (2014).
[46] P. Maris, J. P. Vary, P. Navrátil, W. E. Ormand, H. Nam, and D. J. Dean, Phys. Rev. Lett. **106**, 202502 (2011).
[47] E. Epelbaum, W. Glöckle, and U.-G. Meißner, Nucl. Phys. A **671**, 295 (2000).
[48] P. Büttiker and U.-G. Meißner, Nucl. Phys. A **668**, 97 (2000).
[49] D. R. Entem and R. Machleidt, Phys. Rev. C **68**, 041001 (2003).
[50] A. Ekström *et al.*, Phys. Rev. Lett. **110**, 192502 (2013).
[51] U. van Kolck, Phys. Rev. C **49**, 2932 (1994).
[52] E. Epelbaum, A. Nogga, W. Glöckle, H. Kamada, U.-G. Meißner, and H. Witała, Phys. Rev. C **66**, 064001 (2002).
[53] P. Navrátil, Few-Body Syst. **41**, 117 (2007).
[54] E. Epelbaum, H. Krebs, D. Lee, and U.-G. Meißner, Eur. Phys. J. A **41**, 125 (2009).
[55] D. Gazit, S. Quaglioni, and P. Navrátil, Phys. Rev. Lett. **103**, 102502 (2009).
[56] G. Hagen, T. Papenbrock, A. Ekström, K. A. Wendt, G. Baardsen, S. Gandolfi, M. Hjorth-Jensen, and C. J. Horowitz, Phys. Rev. C **89**, 014319 (2014).
[57] R. Lazauskas, Phys. Rev. C **79**, 054007 (2009).
[58] M. Viviani, A. Deltuva, R. Lazauskas, J. Carbonell, A. C. Fonseca, A. Kievsky, L. E. Marcucci, and S. Rosati, Phys. Rev. C **84**, 054010 (2011).
[59] R. B. Wiringa and S. C. Pieper, Phys. Rev. Lett. **89**, 182501 (2002).
[60] S. C. Pieper, V. R. Pandharipande, R. B. Wiringa, and J. Carlson, Phys. Rev. C **64**, 014001 (2001).
[61] D. Gogny, P. Pires, and R. De Tourreil, Phys. Lett. B **32**, 591 (1970).
[62] M. Bender, P.-H. Heenen, and P.-G. Reinhard, Rev. Mod. Phys. **75**, 121 (2003).
[63] M. Kortelainen, T. Lesinski, J. Moré, W. Nazarewicz, J. Sarich, N. Schunck, M. V. Stoitsov, and S. Wild, Phys. Rev. C **82**, 024313 (2010).
[64] J. Friar and J. Negele, in *Advances in Nuclear Physics*, edited by M. Baranger and E. Vogt (Springer US, New York, 1975), pp. 219–376.
[65] I. Angeli and K. Marinova, At. Data Nucl. Data Tables **99**, 69 (2013).
[66] P. J. Mohr, B. N. Taylor, and D. B. Newell, Rev. Mod. Phys. **84**, 1527 (2012).
[67] A. Ong, J. C. Berengut, and V. V. Flambaum, Phys. Rev. C **82**, 014320 (2010).

[68] R. A. Arndt, I. I. Strakovsky, and R. L. Workman, SAID, Scattering Analysis Interactive Dial-in computer facility, George Washington University (formerly Virginia Polytechnic Institute), solution SM99 (Summer 1999).
[69] M. Wang, G. Audi, A. Wapstra, F. Kondev, M. MacCormick, X. Xu, and B. Pfeiffer, Chin. Phys. C **36**, 1603 (2012).
[70] J. R. Bergervoet, P. C. van Campen, W. A. van der Sanden, and J. J. de Swart, Phys. Rev. C **38**, 15 (1988).
[71] Q. Chen *et al.*, Phys. Rev. C **77**, 054002 (2008).
[72] G. Miller, B. Nefkens, and I. Šlaus, Phys. Rep. **194**, 1 (1990).
[73] R. Machleidt, Phys. Rev. C **63**, 024001 (2001).
[74] A. Huber, T. Udem, B. Gross, J. Reichert, M. Kourogi, K. Pachucki, M. Weitz, and T. W. Hänsch, Phys. Rev. Lett. **80**, 468 (1998).
[75] S. N. More, A. Ekström, R. J. Furnstahl, G. Hagen, and T. Papenbrock, Phys. Rev. C **87**, 044326 (2013).
[76] G. Hagen, T. Papenbrock, M. Hjorth-Jensen, and D. J. Dean, Rep. Prog. Phys. **77**, 096302 (2014).
[77] E. Epelbaum, W. Glöckle, and U.-G. Meißner, Eur. Phys. J. A **19**, 401 (2004).
[78] E. Epelbaum, Prog. Part. Nucl. Phys. **57**, 654 (2006).
[79] G. Hagen, T. Papenbrock, and D. J. Dean, Phys. Rev. Lett. **103**, 062503 (2009).
[80] G. R. Jansen, Phys. Rev. C **88**, 024305 (2013).
[81] A. G. Taube and R. J. Bartlett, J. Chem. Phys. **128**, 044110 (2008).
[82] S. Binder, P. Piecuch, A. Calci, J. Langhammer, P. Navrátil, and R. Roth, Phys. Rev. C **88**, 054319 (2013).
[83] G. Hagen, T. Papenbrock, D. J. Dean, A. Schwenk, A. Nogga, M. Włoch, and P. Piecuch, Phys. Rev. C **76**, 034302 (2007).
[84] R. Roth, S. Binder, K. Vobig, A. Calci, J. Langhammer, and P. Navrátil, Phys. Rev. Lett. **109**, 052501 (2012).
[85] J. F. Stanton and R. J. Bartlett, J. Chem. Phys. **98**, 7029 (1993).
[86] J. R. Gour, P. Piecuch, M. Hjorth-Jensen, M. Włoch, and D. J. Dean, Phys. Rev. C **74**, 024310 (2006).
[87] G. R. Jansen, M. Hjorth-Jensen, G. Hagen, and T. Papenbrock, Phys. Rev. C **83**, 054306 (2011).
[88] J. Shen and P. Piecuch, J. Chem. Phys. **138**, 194102 (2013).
[89] A. Ekström, G. R. Jansen, K. A. Wendt, G. Hagen, T. Papenbrock, S. Bacca, B. Carlsson, and D. Gazit, Phys. Rev. Lett. **113**, 262504 (2014).
[90] I. Shavitt and R. J. Bartlett, *Many-Body Methods in Chemistry and Physics* (Cambridge University Press, Cambridge, 2009).
[91] R. Kanungo, A. Prochazka, M. Uchida, W. Horiuchi, G. Hagen, T. Papenbrock, C. Nociforo, T. Aumann, D. Boutin, D. Cortina-Gil *et al.*, Phys. Rev. C **84**, 061304 (2011).
[92] H. Krebs, A. Gasparyan, and E. Epelbaum, Phys. Rev. C **85**, 054006 (2012).
[93] J. Liu *et al.* (UCNA Collaboration), Phys. Rev. Lett. **105**, 181803 (2010).
[94] A. Gezerlis, I. Tews, E. Epelbaum, M. Freunek, S. Gandolfi, K. Hebeler, A. Nogga, and A. Schwenk, Phys. Rev. C **90**, 054323 (2014).
[95] V. G. J. Stoks, R. A. M. Klomp, M. C. M. Rentmeester, and J. J. de Swart, Phys. Rev. C **48**, 792 (1993).
[96] Y. Akulov and B. Mamyrin, Phys. Lett. B **610**, 45 (2005).
[97] M. Brodeur *et al.*, Phys. Rev. Lett. **108**, 052504 (2012).
[98] R. Sánchez *et al.*, Phys. Rev. Lett. **96**, 033002 (2006).
[99] G. Hupin, S. Quaglioni, and P. Navrátil, arXiv:1412.4101.
[100] F. Ajzenberg-Selove, Nucl. Phys. A **523**, 1 (1991).
[101] R. Firestone, Nucl. Data Sheets **106**, 1 (2005).
[102] R. Firestone, Nucl. Data Sheets **108**, 2319 (2007).
[103] K. Tshoo *et al.*, Phys. Rev. Lett. **109**, 022501 (2012).
[104] K. Emrich and J. Zabolitzky, Nucl. Phys. A **351**, 439 (1981).
[105] C. Barbieri and W. H. Dickhoff, Phys. Rev. C **65**, 064313 (2002).
[106] B. A. Brown and W. A. Richter, Phys. Rev. C **74**, 034315 (2006).
[107] S. K. Bogner, H. Hergert, J. D. Holt, A. Schwenk, S. Binder, A. Calci, J. Langhammer, and R. Roth, Phys. Rev. Lett. **113**, 142501 (2014).
[108] G. R. Jansen, J. Engel, G. Hagen, P. Navratil, and A. Signoracci, Phys. Rev. Lett. **113**, 142502 (2014).
[109] L. Caceres *et al.*, arXiv:1501.01166.
[110] P.-G. Reinhard, J. Piekarewicz, W. Nazarewicz, B. K. Agrawal, N. Paar, and X. Roca-Maza, Phys. Rev. C **88**, 034325 (2013).
[111] H. DeVries, C. W. DeJager, and C. DeVries, At. Data Nucl. Data Tables **36**, 494 (1987).
[112] L. Coraggio, J. W. Holt, N. Itaco, R. Machleidt, L. E. Marcucci, and F. Sammarruca, Phys. Rev. C **89**, 044321 (2014).
[113] D. Vautherin and D. M. Brink, Phys. Rev. C **5**, 626 (1972).